

COMPUTATIONAL ANALYSIS OF A MULTISTAGE AXIAL COMPRESSOR

by

CHAITHANYA MAMIDOJU

Presented to the Faculty of the Graduate School of
The University of Texas at Arlington in Partial Fulfillment
of the Requirements
for the Degree of

MASTER OF SCIENCE IN AEROSPACE ENGINEERING

THE UNIVERSITY OF TEXAS AT ARLINGTON

May 2014

Copyright © by CHAITHANYA MAMIDOJU 2014
All Rights Reserved

To my parents Vanisri and Srinivas Mamidoju
and my brother Kranthi Kumar.

ACKNOWLEDGEMENTS

I express my deep gratitude to my thesis supervisor and mentor Dr. Brian H Dennis for putting a lot of faith in me and making me feel that I always belonged here. If only I could achieve half the amount of work he does in a day I would be happy. Doing research and coursework with him has taught me a lot, especially approaching a problem and coming up with new ideas.

I am deeply honored and privileged to have two stalwarts of the Mechanical and Aerospace Department, Dr. Zhen Xue Han and Dr. Bo P Wang in my committee.

I would like to thank my love Yashwanth M Swamy for continuous support and encouragement throughout my Masters study. I am also grateful to my friends Shilpa Andam, Mahesan Revathi Sanjay, Ravi Kiran Paturi for for sticking with me through thick and thin. I would also like to thank all my close friends at UTA for taking the responsibility of being my local guardians.

Finally, I am thankful to my CFD lab colleagues for being with me and for their valuable inputs. I would also like to thank my well-wishers for their love and support. I am also grateful to all my past and present teachers who have played a stellar role in shaping up my career.

Above all, I would like to express my deepest gratitude to my parents Srinivas Mamidoju and Vani Sri Mamidoju, to whom I owe my existence and to my brother Kranthi Kumar Mamidoju for moral support. They cherished my highs, pulled me out of the lows, but most importantly, they made me a good human being.

April 21, 2014

ABSTRACT

COMPUTATIONAL ANALYSIS OF A MULTISTAGE AXIAL COMPRESSOR

CHAITHANYA MAMIDOJU, M.S.

The University of Texas at Arlington, 2014

Supervising Professor: Brian H Dennis

Turbomachines are used extensively in Aerospace, Power Generation, and Oil & Gas Industries. Efficiency of these machines is often an important factor and has led to the continuous effort to improve the design to achieve better efficiency. The axial flow compressor is a major component in a gas turbine with the turbine's overall performance depending strongly on compressor performance. Traditional analysis of axial compressors involves throughflow calculations, isolated blade passage analysis, Quasi-3D blade-to-blade analysis, single-stage (rotor-stator) analysis, and multi-stage analysis involving larger design cycles.

In the current study, the detailed flow through a 15 stage axial compressor is analyzed using a 3-D Navier Stokes CFD solver in a parallel computing environment. Methodology is described for steady state (frozen rotor stator) analysis of one blade passage per component. Various effects such as mesh type and density, boundary conditions, tip clearance and numerical issues such as turbulence model choice, advection model choice, and parallel processing performance are analyzed. A high sensitivity of the predictions to the above was found. Physical explanation to the flow features

observed in the computational study are given. The total pressure rise verses mass flow rate was computed.

TABLE OF CONTENTS

ACKNOWLEDGEMENTS	iv
ABSTRACT	v
LIST OF ILLUSTRATIONS	ix
LIST OF TABLES	xi
Chapter	Page
1. Introduction	1
1.1 Motivation	1
1.2 Objective	2
1.3 Outline	3
2. Computational Fluid Dynamics	4
2.1 Governing Equations	5
2.1.1 Conservation of Mass	6
2.1.2 Conservation of Momentum	6
2.1.3 Conservation of Energy	6
2.2 Turbulence modelling and y-plus	7
2.2.1 $k - \epsilon$ Model	8
2.2.2 Shear Stress Transport model	9
2.3 Finite Volume Method	11
2.4 Software validation	11
3. Axial Flow Compressors	14
4. Methodology	16
4.1 Analysis type	16

4.2	Parallel Processing	19
4.2.1	Partitioning step	19
4.2.2	Running step	20
4.3	Preliminary studies	21
4.3.1	Turbulence Modelling	21
4.3.2	Meshing	23
4.4	Computational study using three climatic conditions	24
5.	Results and Discussions	26
5.1	Outlet Static Pressure of 180 kPa for three climatic conditions	26
5.2	Outlet Static Pressure of 180 kPa, 270 kPa and 300 kPa for winter condition	28
6.	Concluding Remarks	35
6.1	Future work	36
Appendix		
A.	INPUT CODE FOR PARALLEL PROCESSING	37
REFERENCES		39
BIOGRAPHICAL STATEMENT		41

LIST OF ILLUSTRATIONS

Figure	Page
1.1 Aeolipile developed by Hero of Alexandria 120 BC	1
1.2 48-Stage Axial Flow Compressor made by Parsons in 1904	2
1.3 Westinghouse J-30 'yankee' 10-stage Axial Flow Compressor [1]	3
2.1 Hub-to-tip and blade-to-blade stream surfaces	4
2.2 Subdivisions of the near-wall region [6]	10
2.3 Plot of Total Pressure ratio and Normalized mass flow of Experimental Analysis [7]	12
2.4 Plot of Total Pressure ratio and Normalized mass flow of Computational Analysis	13
3.1 A typical multistage axial flow compressor (Rolls-Royce, 1992) [8]	14
3.2 Pressure and velocity profiles (Rolls-Royce, 1992) [8]	15
4.1 Meridional view of 15 stage compressor	17
4.2 Flynn's Taxonomy [10]	18
4.3 Bisection type mesh partitioning [?]	20
4.4 Parallel computers in CFD lab at UTA	21
4.5 Eddy Viscosity of the compressor using $\kappa - \epsilon$ turbulence model	22
4.6 Eddy Viscosity of the compressor using SST turbulence model	22
4.7 Plot of Total Pressure Ratio to Mass Flow Rate	23
4.8 Topology at Mid-span of a Rotor	24
5.1 360 degree view of the compressor	26
5.2 Graph of Total Pressure Ratio versus Stage Number	27

5.3	Pressure contour at 50 percent mid span for Exit Static Pressure = 180 kPa in winter	28
5.4	Pressure contour at 50 percent mid span for Exit Static Pressure = 180 kPa in average climate	29
5.5	Pressure contour at 50 percent mid span for Exit Static Pressure = 180 kPa in summer	29
5.6	Velocity Vector plot at 50 percent mid span for Exit Static Pressure = 180 kPa in winter	30
5.7	Velocity vector plot at 50 percent mid span for Exit Static Pressure = 180 kPa in average climate	30
5.8	Velocity vector plot at 50 percent mid span for Exit Static Pressure = 180 kPa in summer	31
5.9	Graph of Total Pressure Ratio versus Stage Number for winter condition	32
5.10	Graph of Total Pressure Ratio versus mass flow rate for winter condition	33
5.11	Pressure contour at 50 percent mid span for Exit Static Pressure = 270 kPa in winter	33
5.12	Velocity vector plot at 50 percent mid span for Exit Static Pressure = 270 kPa in winter	34

LIST OF TABLES

Table		Page
4.1	Number of Blades of Rotor and Stator	17
4.2	Total Pressure ratio and computational time for y-plus values and number of nodes	25
4.3	Boundary conditions of 3 climatic conditions	25
5.1	Overall Total Pressure ratio and Inlet mass flow rate for three climatic conditions	27

CHAPTER 1

Introduction

1.1 Motivation

Turbomachines are used extensively in Aerospace, Power Generation, and Oil and Gas Industries. Efficiency of these machines is often an important factor and has led to the continuous effort to improve the design to achieve better efficiency. From the man's beginning to 1700 AD, all the motive power was provided by men or animals. One of the earliest use of Turbomachinery is attributed to Hero of Alexandria, 100 BC, where in his book Pneumatics, described a devise known as Aeolipile, fig 1.1, which rotates using the reaction principle [1].



Figure 1.1. Aeolipile developed by Hero of Alexandria 120 BC.

Thereafter, there has been rapid growth of technology in hydraulic turbines, steam engines, and steam and gas turbines, with continuous development in the de-

sign of turbomachinery components such as compressors, turbines and fans. First patent of a multistage axial flow compressor was obtained by Sir Charles Parsons fig 1.2 in 1884 which consisted of 48 stages but eventually had to abandon due to lack of aerodynamic. The period during and after World War II has seen new aerodynamically efficient engines consisting of multistage axial flow compressors such as 'J-30 Yankee' designed by Westinghouse, used in the McDonnell Douglas FH-1 Phantom fig 1.3.

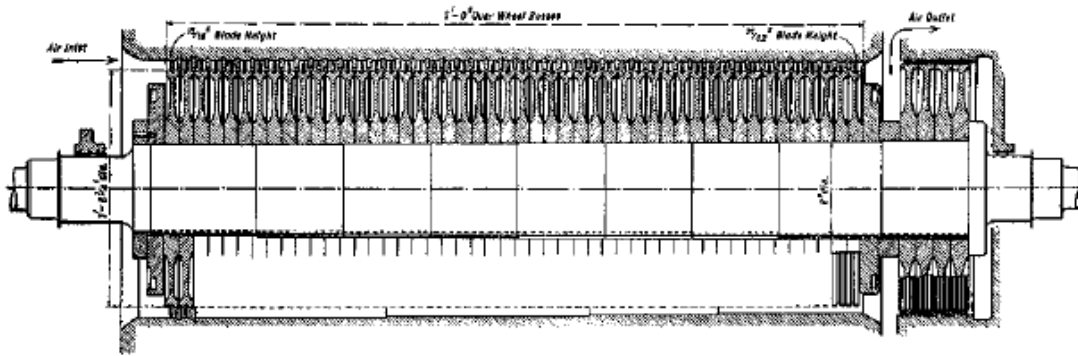


Figure 1.2. 48-Stage Axial Flow Compressor made by Parsons in 1904.

1.2 Objective

The objective of the study is to analyze the flow through a multi-stage axial compressor by optimizing critical parameters both within the solver (CFD tool) and the control volume of the compressor. As part of preliminary analysis, generate an effective grid by varying y-plus and number of nodes in the O-grid region and To carryout a comparative study between k-epsilon and SST turbulence models to improve the end result. By using the resulting turbulence model and grid, analyze the

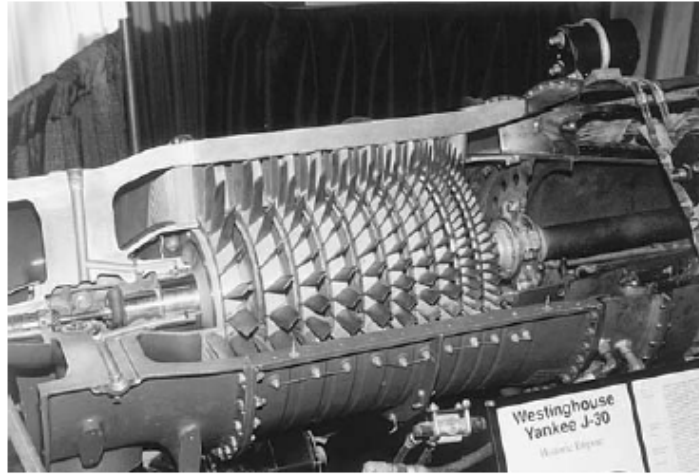


Figure 1.3. Westinghouse J-30 "yankee" 10-stage Axial Flow Compressor [1].

total pressure ratio for three climatic conditions. The computing results are validated using the actual data of an existing compressor.

1.3 Outline

The thesis work presented analyzes the flow through a multi-stage axial flow compressor using CFD tool, ANSYS CFX 14.5. The basics of Computational Fluid Dynamics for Turbomachinery is described in Chapter 2. Chapter 3 gives basics of Axial Flow Compressors. The methodology, with preliminary analysis of turbulence model and grid sensitivity are presented in Chapter 4. Chapter 5 discusses the results of flow analysis for various climatic conditions and exit static pressures. The concluding remarks are layed out in Chapter 6.

CHAPTER 2

Computational Fluid Dynamics

Computational Fluid Dynamics, commonly known as CFD, is a method of solving the governing equations of a fluid flow using numerical techniques and computing power. When compared to traditional methods, such as wind tunnel tests that involve destructive testing, numerical analysis is much faster, cost effective and feasible. The usage of these numerical techniques is comparatively higher in the design of Turbomachinery than in any other field. The application of the same, dates back to 1940s with the introduction of blade-to-blade (S1) and hub-to-tip (S2) stream surfaces by Wu [2].

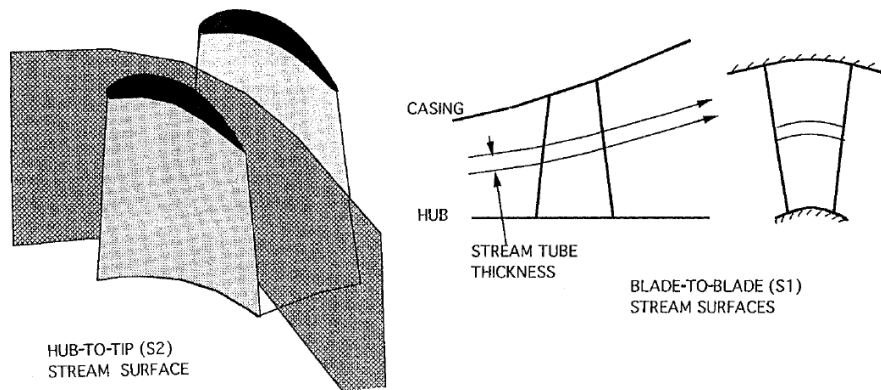


Figure 2.1. Hub-to-tip and blade-to-blade stream surfaces [3].

These two stream surfaces are shown in fig 2.1, where hub-to-tip stream surface (S2) is defined as axisymmetric flow mean stream surfaces and blade-to-blade stream surface (S1) is untwisted surface of revolution. S1 stream surface is the basis for

blade design and S2 stream surface is used called as 'throughflow calculations' which is the backbone of turbomachinery design. In [3], they pointed out the importance of throughflow calculations and the streamline curvature method which acted as a base for the calculation of mass flow rate by taking pressure ratio as one of the inputs. One weakness in thoroughflow calculations was the inability to predict the recirculating flows. This is overcome by including the effects of Three Dimensional flows to the throughflow calculation which gives more accurate results. The above mentioned numerical methods, which are inviscid and should be coupled with boundary layer calculations, are replaced by the direct solution of the Navier-Stokes (N-S) Equations which include calculation of boundary layer calculation in them.

CFD analysis is a step by step process which begins defining the equations for the fluid flow. These are the equations of conservation of mass, momentum and energy in partial differential equation form, followed by discretisation of the domain and defining boundary conditions. Discretization of the domain involves breaking up the required area or volume into smaller areas or volumes over which the governing equations are applied. The equations are applied to the smaller volumes using Control Volume Method.

2.1 Governing Equations

Governing Equations are the mathematical statements of the three basic physical flows which are (i) Mass is conserved, (ii) Newton's second Law ($\mathbf{F} = m\mathbf{a}$) and (iii) Energy is conserved. Depending on the type of problem, equation of state and species conservation (in case of reacting flows) are also used. In compressor analysis, the engineering quantities such as velocity, pressure, temperature are evaluated, considering the effect of turbulence. In order to adequately define the flow characteristics, the governing equations must consist of fluid flow, energy and turbulence

models. Descriptions of the equations used and an explanation of how these are applied is explained below. For the derivations of each equation, refer to [4]

2.1.1 Conservation of Mass

Conservation of mass is based on the theory that mass is neither created nor destroyed. This theory is applied to a three-dimensional control volume to obtain conservation equation in 3-dimensional, unsteady, compressible form.

$$\frac{\partial \rho}{\partial t} + \frac{\partial (\rho u)}{\partial x} + \frac{\partial (\rho v)}{\partial y} + \frac{\partial (\rho w)}{\partial z} = 0 \quad (2.1.1)$$

2.1.2 Conservation of Momentum

Momentum equations are derived from Newton's Second Law of Motion which states that forces on a fluid volume should be balanced. The equations derived for momentum are listed below which give the transfer of momentum through a 3-dimensional, compressible, unsteady field.

$$\frac{\partial (\rho u)}{\partial t} + \frac{\partial (\rho u^2)}{\partial x} + \frac{\partial (\rho uv)}{\partial y} + \frac{\partial (\rho uw)}{\partial z} = -\frac{\partial p}{\partial x} + \mu \frac{\partial^2 u}{\partial x^2} + \mu \frac{\partial^2 u}{\partial y^2} + \mu \frac{\partial^2 u}{\partial z^2} + S_x \quad (2.1.2)$$

$$\frac{\partial (\rho v)}{\partial t} + \frac{\partial (\rho uv)}{\partial x} + \frac{\partial (\rho v^2)}{\partial y} + \frac{\partial (\rho vw)}{\partial z} = -\frac{\partial p}{\partial y} + \mu \frac{\partial^2 v}{\partial x^2} + \mu \frac{\partial^2 v}{\partial y^2} + \mu \frac{\partial^2 v}{\partial z^2} + S_y \quad (2.1.3)$$

$$\frac{\partial (\rho w)}{\partial t} + \frac{\partial (\rho uw)}{\partial x} + \frac{\partial (\rho vw)}{\partial y} + \frac{\partial (\rho w^2)}{\partial z} = -\frac{\partial p}{\partial z} + \mu \frac{\partial^2 w}{\partial x^2} + \mu \frac{\partial^2 w}{\partial y^2} + \mu \frac{\partial^2 w}{\partial z^2} + S_z \quad (2.1.4)$$

2.1.3 Conservation of Energy

The Conservation of Energy equation is derived from the First Law of Thermodynamics which states that the time rate of change of energy is the sum of net rate of heat added and net rate of work done on the system. When this law is applied to a 3-dimensional control volume, using Fourier's law of heat conduction, Tu et al [5] derived the 3-dimensional conservation of energy equation.

$$\frac{\partial T}{\partial t} + \frac{\partial uT}{\partial x} + \frac{\partial vT}{\partial y} + \frac{\partial wT}{\partial z} = \frac{k}{\rho C_p} \left[\frac{\partial^2 T}{\partial x^2} + \frac{\partial^2 T}{\partial y^2} + \frac{\partial^2 T}{\partial z^2} \right] + \frac{1}{\rho C_p} \frac{\partial p}{\partial t} + \frac{\Phi}{\rho C_p} \quad (2.1.5)$$

The effects on energy due to viscous stresses are represented by the dissipation function (Φ). The function represents a source of energy due to the deformation work done on the fluid that is converted into energy. Using Newton's Law of viscosity, the shear stresses on the control volume can be converted into velocity gradients and the dissipation function is expressed as:

$$\begin{aligned} \Phi = & \left(\frac{\partial u\tau_{xx}}{\partial x} \right) + \left(\frac{\partial u\tau_{yx}}{\partial y} \right) + \left(\frac{\partial u\tau_{zx}}{\partial z} \right) + \left(\frac{\partial v\tau_{xy}}{\partial x} \right) + \left(\frac{\partial v\tau_{yy}}{\partial y} \right) + \left(\frac{\partial v\tau_{zy}}{\partial z} \right) + \\ & \left(\frac{\partial w\tau_{xz}}{\partial x} \right) + \left(\frac{\partial w\tau_{yz}}{\partial y} \right) + \left(\frac{\partial w\tau_{zz}}{\partial z} \right) \end{aligned} \quad (2.1.6)$$

2.2 Turbulence modelling and y-plus

Turbulence is a fundamental aspect of most engineering problems in CFD. It is described as a irregular flow condition in which the various quantities such as velocity, pressure show random variation with space and time. Turbulence can be visualized by rotational motion commonly referred to as turbulent eddies. Rotational motion of the flow or turbulent eddies, are defined over a wide range of length scales. Length scales represent the size of turbulent eddies and are dependent on the size of the model and Reynolds number. In order to enable the effects of turbulence to be predicted, extensive CFD research has concentrated on methods that make use of turbulence models. Turbulence models are used to predict the effects of turbulence in fluid flow without resolving all scales of the smallest turbulent fluctuations. A number of models have been developed that can be used to approximate turbulence based on the Reynolds Averaged Navier-Stokes (RANS) Equations.

2.2.1 $k - \epsilon$ Model

$k - \epsilon$ turbulence model is a type of eddy viscosity model where k is the turbulence kinetic energy and is defined as the variance of the fluctuations in velocity where as ϵ is the turbulence eddy dissipation. This model introduces two new variables into the system of equations and the continuity equation is then :

$$\frac{\partial \rho}{\partial t} + \frac{\partial}{\partial x_j} (\rho U_j) = 0 \quad (2.2.1)$$

and the momentum equation becomes:

$$\frac{\partial \rho U_i}{\partial t} + \frac{\partial}{\partial x_j} (\rho U_i U_j) = -\frac{\partial p'}{\partial x_i} + \frac{\partial}{\partial x_j} \left[\mu_{eff} \left(\frac{\partial U_i}{\partial x_j} + \frac{\partial U_j}{\partial x_i} \right) \right] + S_M \quad (2.2.2)$$

where S_M is the sum of body forces, μ_{eff} is the effective viscosity accounting for turbulence, and p' is the modified pressure. We know from the eddy viscosity concept that:

$$\mu_{eff} = \mu + \mu_t \quad (2.2.3)$$

where μ_t is the turbulence viscosity and the $k - \epsilon$ model assumes μ_t as:

$$\mu_t = C_\mu \rho \frac{k^2}{\epsilon} \quad (2.2.4)$$

where C_μ is a constant. The values of the k and ϵ come from the differential transport equations for the turbulence kinetic energy and turbulence dissipation rate:

$$\frac{\partial (\rho k)}{\partial t} + \frac{\partial}{\partial x_j} (\rho U_j k) = \frac{\partial}{\partial x_j} \left[\left(\mu + \frac{\mu_t}{\sigma_k} \right) \frac{\partial k}{\partial x_j} \right] + P_k - \rho \epsilon + P_{kb} \quad (2.2.5)$$

$$\frac{\partial (\rho \epsilon)}{\partial t} + \frac{\partial}{\partial x_j} (\rho U_j \epsilon) = \frac{\partial}{\partial x_j} \left[\left(\mu + \frac{\mu_t}{\sigma_\epsilon} \right) \frac{\partial \epsilon}{\partial x_j} \right] + \frac{\epsilon}{k} (C_{\epsilon 1} P_k - C_{\epsilon 2} \rho \epsilon + C_{\epsilon 1} P_{\epsilon b}) \quad (2.2.6)$$

where $C_{\epsilon 1}$, $C_{\epsilon 2}$, σ_k and σ_ϵ are constants.

2.2.2 Shear Stress Transport model

The Shear Stress Transport model is type of $k - \omega$ model where k gives turbulent kinetic energy and ω gives specific dissipation. ω determines the scale of the turbulence where as k determines the energy in the turbulence. The use of a $k - \omega$ formulation in the inner parts of the boundary layer makes the model directly usable all the way down to the wall through the viscous sub-layer, hence the SST $k - \omega$ model can be used as a Low-Re turbulence model without any extra damping functions. The SST formulation also switches to a $k - \epsilon$ behavior in the free-stream and thereby avoids the common $k - \omega$ problem that the model is too sensitive to the inlet free-stream turbulence properties. Since this model accounts for the transport of the turbulent shear stress, it gives highly accurate predictions of the onset and the amount of flow separation under adverse pressure gradients.

Turbulence modelling in this study is a fluid flow is closely associated with y^+ , dimensionless distance from the wall. The near wall region can be subdivided into two layers as shown in fig 2.2. In the innermost viscous sublayer, the flow is almost laminar and viscous force plays dominant role. Further away from the wall, in the logarithmic sublayer, turbulence dominates the mixing process. Assuming that the logarithmic layer approximates the velocity distribution near the wall, the fluid shear stress as a function of velocity at a distance from the wall can be calculated, and is known as wall function.

The logarithmic relation for the near wall velocity is given by :

$$u^+ = \frac{U_t}{u_\tau} = \frac{1}{\kappa} \ln(y^+) + C \quad (2.2.7)$$

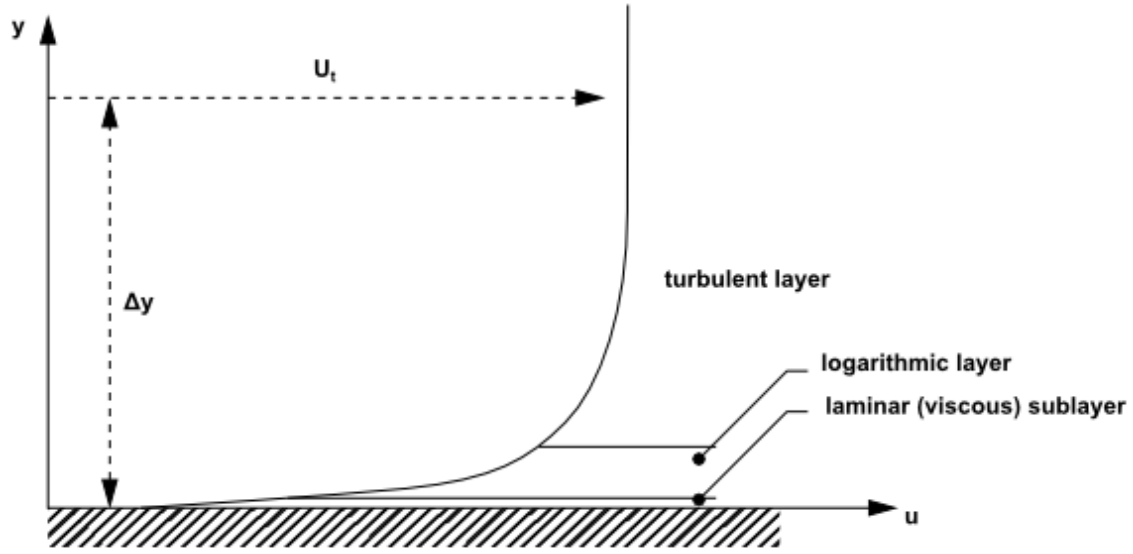


Figure 2.2. Subdivisions of the near-wall region [6].

where :

$$y^+ = \frac{\rho \Delta y u_\tau}{\mu} \quad (2.2.8)$$

$$u_\tau = \left(\frac{\tau_\omega}{\rho} \right) \quad (2.2.9)$$

u^+ is the near wall velocity, u_τ is the friction velocity, U_t is the known velocity tangent to the wall at the distance Δy from the wall, y^+ is the dimensionless distance from the wall, τ_ω is the wall shear stress, κ is the von Karman constant and C is the log-layer constant depending on wall roughness. The definition for the Yplus variable that is used in the post processing of ANSYS CFX is given as

$$y^+ = \frac{\sqrt{\tau_\omega/\rho} \cdot \Delta n}{\nu} \quad (2.2.10)$$

where Δn is the distance between the first and second grid points off the wall.

2.3 Finite Volume Method

Once the governing equations are defined, the domain is discretized for the equations to be applied. The Finite Volume Method (FVM) is the most widely applied method in CFD. The FVM discretizes the governing equations directly in the physical space. Since this method works with the control volume and not the grid intersection points, it can accommodate any type of grid, structured or unstructured. The conservation equations are integrated over each control volume, and Gauss' Divergence Theorem is applied to evaluate cell centered values from values at the cell faces. The variable values at the cell faces are averaged values from the adjacent cell centers (First-Order Upwind) or the adjacent two cells (Second Order Upwind). Since the discrete equations are more diffuse than the original differential equations, the First Order Upwinding Method (FOU) introduces some numerical diffusion and even more where large gradients exist. However, the FOU method converges faster than SOU methods and can be used with higher Courant Numbers to increase convergence rates. The FOU scheme is utilized in this analysis since it is a design analysis and the convergence rate (or time) is a major factor in retrieving a design solution. Refer to Tu, et al [5] for more information.

2.4 Software validation

In order to validate the accuracy of CFX software, the same type of grid and boundary conditions in pre-processing are implemented on the analysis of Rotor 37 which is a 36 blade single stage rotor, whose experimental data is vastly available. By varying the input mass flow rates, a set of simulations were performed. From the obtained results, Total pressure ratio to the mass flow rate normalized by the choking massflow, m_{max} , where $m_{max} = 20.93 \pm 0.14 kg/sec$, is plotted. The variation of the

plot gave an agreement with the experimental data. The Rotor stall is encountered at $\dot{m}/\dot{m}_{max} = 0.919$ in the experimental data where as in the study it was seen at 0.92 as shown in the fig 2.3 and fig 2.4

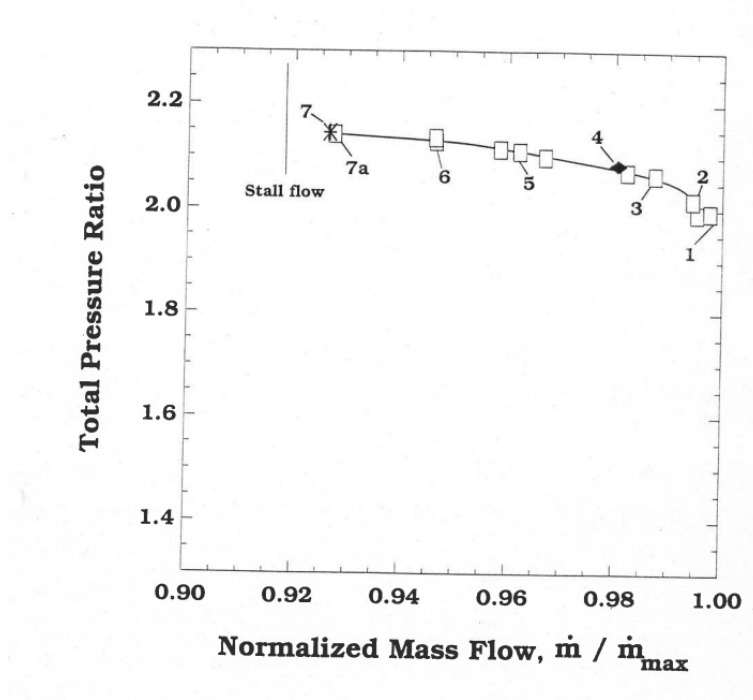


Figure 2.3. Plot of Total Pressure ratio and Normalized mass flow of Experimental Analysis [7].

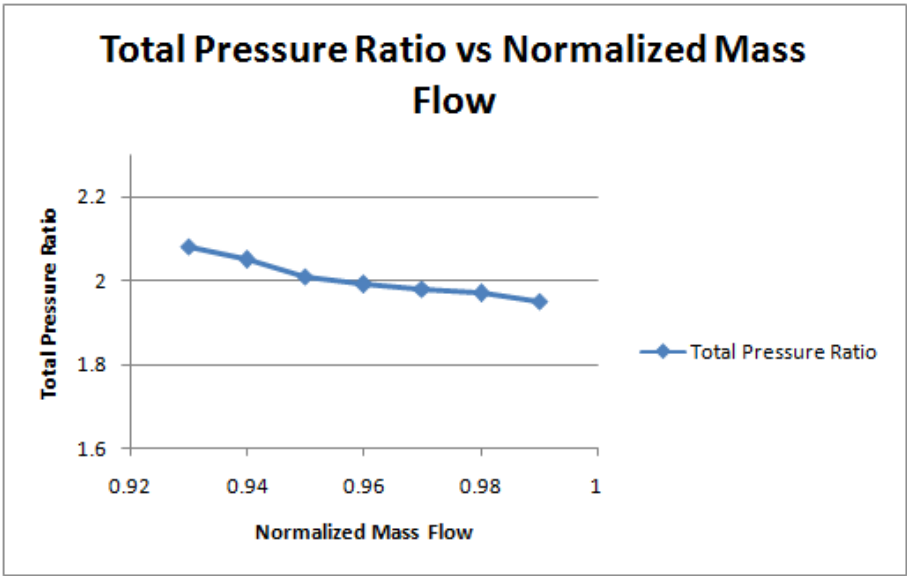


Figure 2.4. Plot of Total Pressure ratio and Normalized mass flow of Computational Analysis.

CHAPTER 3

Axial Flow Compressors

An Axial Flow compressors is typically made of alternating rows of rotors (rotating blades) and stators (stationary blades) as shown in fig 3.1. The first stationary row is called inlet guide vanes or IGV. Each successive rotor-stator pair is called a compressor stage.

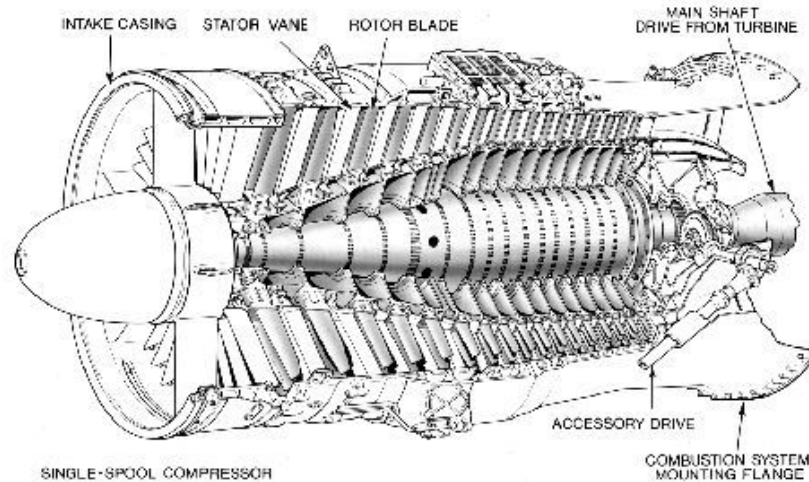


Figure 3.1. A typical multistage axial flow compressor (Rolls-Royce, 1992) [8].

The working of a compressor is based on the energy exchanges. Consider the Bernoulli Equation, where P_T is the stagnation pressure, a measure of the total energy carried in the flow, p is the static pressure, a measure of the internal energy, and the velocity terms, a measure of kinetic energy associated with three components of velocity, u is radial, v is tangential, w is axial.

$$P_T = p + \frac{1}{2}\rho(u^2 + v^2 + w^2) \quad (3.0.1)$$

The rotor adds swirl to the flow, increasing the total energy carried in the flow by increasing angular momentum. The stator removes the swirl from the flow without adding energy to the flow since it is stationary. The stator rather converts the kinetic energy associated with the swirl to internal energy increasing the static pressure of the flow. The typical velocity and pressure profiles are shown in fig 3.2

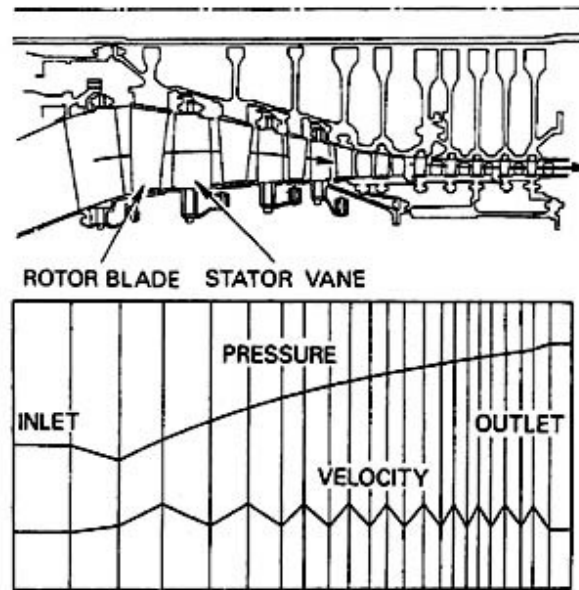


Figure 3.2. Pressure and velocity profiles (Rolls-Royce, 1992) [8].

CHAPTER 4

Methodology

Computational Fluid Dynamics has been used to analyze the flow through rotating machines in general and axial compressors particularly. In current study, a 15 stage axial flow compressor is analyzed using commercial CFD package CFX 14.5 which has integrated pre and post processing capabilities. The compressor consists of 31 blade rows, with an inlet guide vane (IGV) used for blast furnace [9]. The compressor flow path is that of a constant diameter. The hub-tip radius ratio ranges from 0.615 at the inlet blade to 0.798 at the outlet blade. The airfoils of all the 31 blade rows belong to NACA 65-series and the rotor blades have constant airfoil shape from hub to tip. The number of blades in each row of rotor and stator are given in the Table 4.1. The IGV, first and second stage stator constitutes of twisted blades while the rest are straight as shown in fig 4.1.

A 3D Navier Stokes solver, Ansys CFX [6] is used to analyse. The flow solver consists of three stages. The pre-processing where, geometry, mesh, boundary conditions are set. The defined file is then solved using serial or a parallel solver and once the solver converges, the results file is then analysed in post- processing segment.

4.1 Analysis type

Steady State analysis where model flows do not change with time is carried out in this study. Here the steady conditions are assumed to have been reached after a relatively long interval. Frozen rotor simulations are implemented where rotating and stationary parts have a fixed relative position. This type of simulation is also

Table 4.1. Number of Blades of Rotor and Stator

Rotor	Number of Blades	Stator	Number of Blades
		0	28
1	27	1	28
2	27	2	36
3	33	3	30
4	31	4	30
5	31	5	26
6	37	6	26
7	37	7	28
8	37	8	36
9	37	9	36
10	47	10	36
11	47	11	36
12	47	12	36
13	47	13	36
14	47 <td>14</td> <td>36</td>	14	36
15	47	15	36

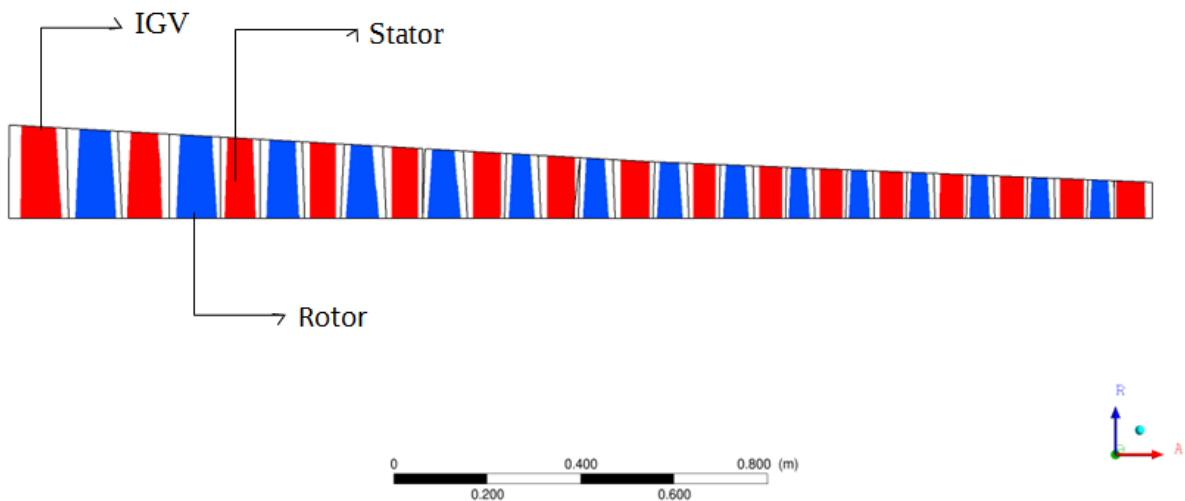


Figure 4.1. Meridional view of 15 stage compressor.

called multiple frame of reference approach where a frame transformation is done to include the rotating effect on the rotating sections. With a frozen-rotor simulation rotating wakes, secondary flows, leading edge pressure increases etc will always stay in exactly the same positions which makes the simulation dependent on exactly how the rotors and the stators are positioned. When compared to mixing plane approach where a coupling between tangential averages on both sides of the interface between rotor and stator is done, a frozen rotor approach provides a local coupling imposing the local flow conditions from one row to the other.

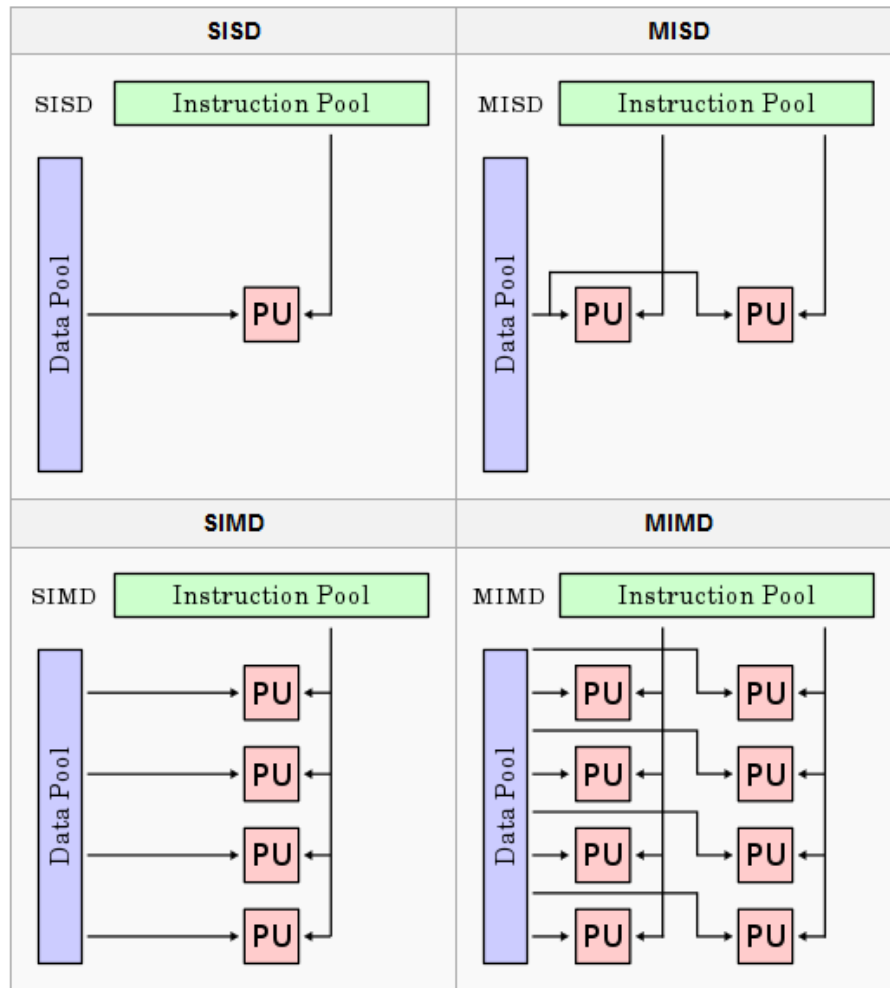


Figure 4.2. Flynn's Taxonomy [10].

4.2 Parallel Processing

Complex flow fields in turbomachine require high performance computer to solve governing equations to meet memory, cost and time constraints. Parallel computing is the simultaneous operation of multiple computational tasks on a computer system. It has been an integral part of computing system from their beginning with the earliest reference appears to be the description by L. Menabrea of Charles Babbages computer [11]. For many years the taxonomy of Flynn has been used for the classification of high performance computers.[12]. This classification is based on the way instruction and data streams are handled. The classification is shown in fig 4.2.SISD refers to Single Instruction Single Data Stream, the class of a traditional computer like PC. SIMD is the Single Instruction Multiple Data Stream type architecture which is implemented by the solver used in research. This model runs identical versions of the code on one or more processors. The third type is MISD which is Multiple Instruction Single Data Stream type, used in Space Shuttle flight control computer. Parallel processing is explained with respect to CFX solver. The overall parallel run procedure is divided in two two categories : (1) Partitioning step and (2) Running step.

4.2.1 Partitioning step

Partitioning is the process of dividing the mesh into a number of partitions each of which may be solved by a separate processor. Several partitioning methods have been developed, but most are based on recursive bisection and differ only in the bisection step. The original mesh is first decomposed into two meshes of approximately equal size. The decomposition is then repeated recursively until the required number of partitions is obtained. The fig 4.3 describes the process. MeTiS Partitioning model based on multilevel k-way algorithm are implemented in current study.

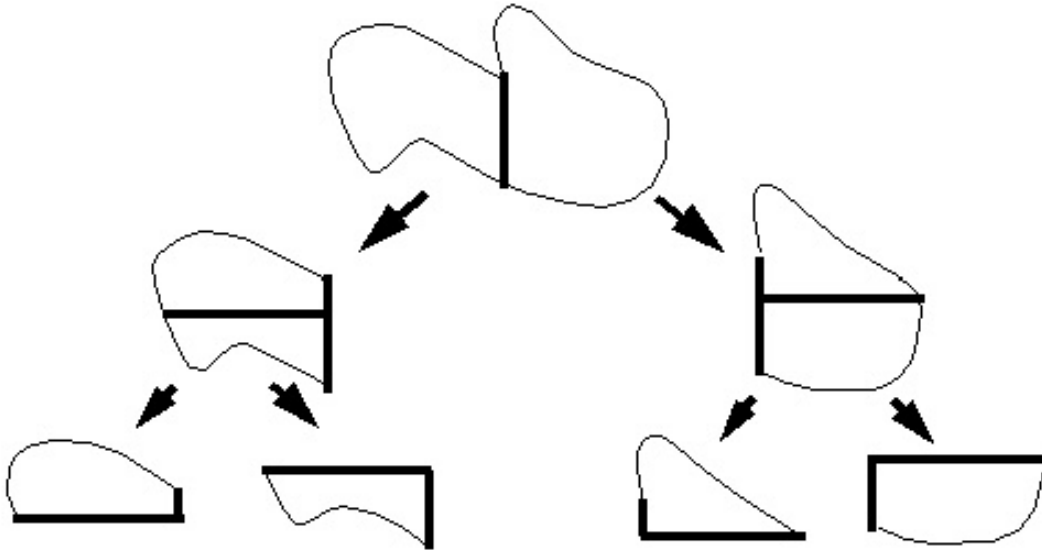


Figure 4.3. Bisection type mesh partitioning [6].

4.2.2 Running step

A running step is where the mesh partitions are solved using separate processes (a master and one or more slave partitions), with each process working on its own partition. Simulation control and user interaction, as well as the input/output phases of parallel run are performed by master process. This approach guarantees good parallel performance and scalability of the parallel code. Communication between processes during parallel run is performed using PVM (Parallel Virtual Machine) or MPI (Message Passing Interface) libraries. For homogeneous distributed machines and multi-processor machines, MPI has been shown to give improved parallel efficiency over the PVM libraries. Detailed information can be obtained in any Parallel Computing texts books.

The parallel computers fig 4.4 available in Computational Fluid Dynamics Laboratory of University of Texas at Arlington are used for the analysis. There are a total of nine nodes, each consisting of four cores. The Linux operating system is used



Figure 4.4. Parallel computers in CFD lab at UTA.

on all the machines. The code to submit files can be found in the appendix. For all the computations, a physical timescale of $\frac{0.1}{\omega}$ is used, where ω is the rotational speed of the compressor in radians per second. The residual value of $1E-5$ is used for the convergence criteria and the number of iterations set for the solver is 400.

4.3 Preliminary studies

4.3.1 Turbulence Modelling

The key problem of accurate numerical simulation of complex flows is the description of turbulence. A large amount of CFD research on turbomachinery has concentrated on methods which make use of turbulence models. There is no single model which is suitable to all types of simulations. In order to accurately predict more difficult cases, like separating flows, rotating flows, flows strongly affected by secondary flows etc. it is often necessary to use a more refined turbulence model. Common choices are two-equation models like the model. In this research particularly, a comparison between k-epsilon and SST model is carried out. The fig 4.5 & fig 4.6 gives Eddy Viscosity contour plot for both the turbulence models.

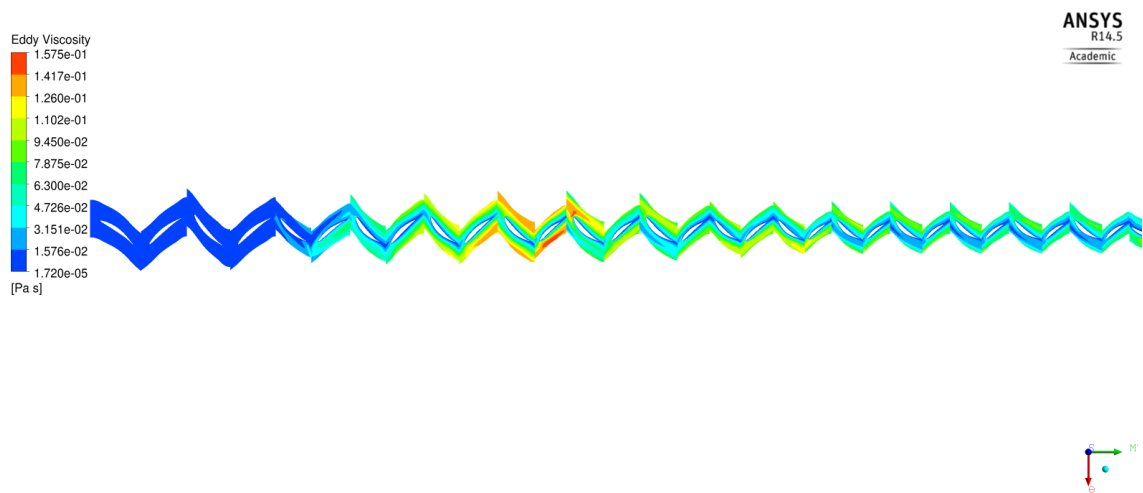


Figure 4.5. Eddy Viscosity of the compressor using $\kappa - \epsilon$ turbulence model.

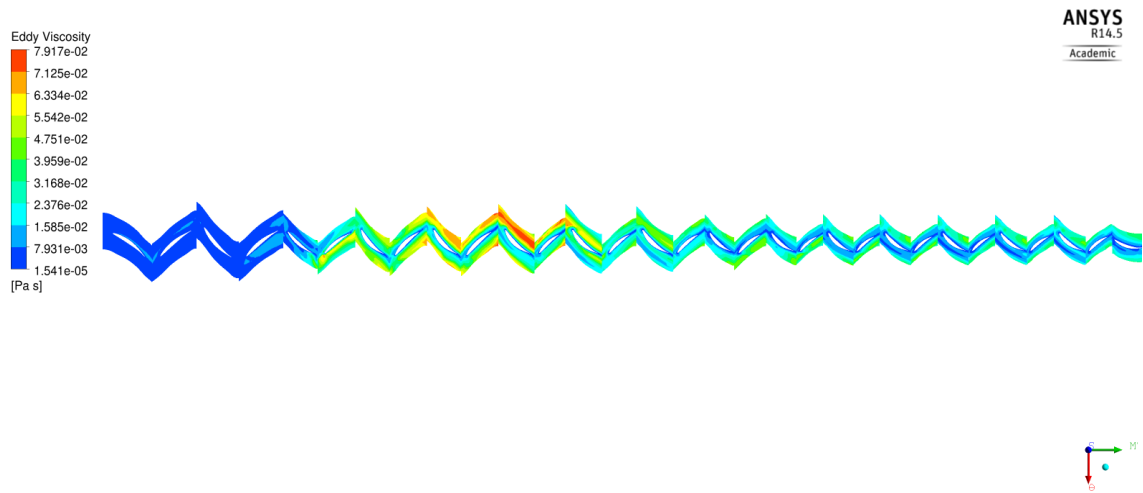


Figure 4.6. Eddy Viscosity of the compressor using SST turbulence model.

A better variation of Eddy viscosity is obtained by using SST model and the fig 4.7 shows the variation in total pressure ratio obtained for different types of grid, using SST model when compared to k-epsilon model.

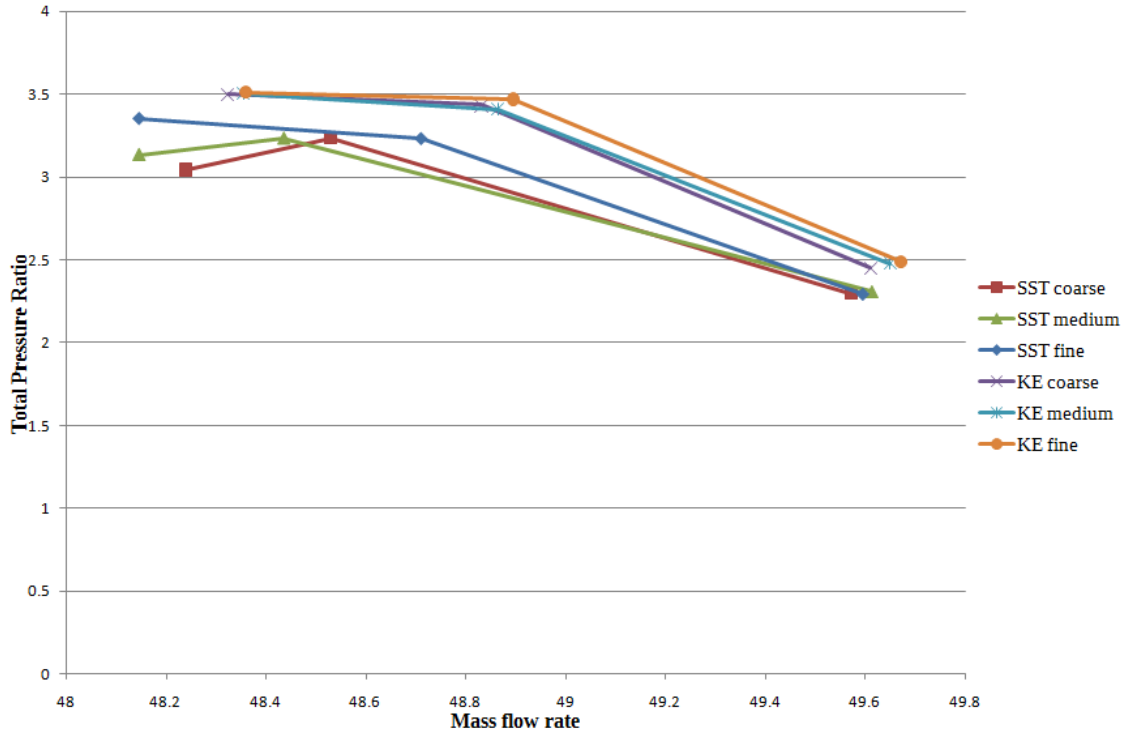


Figure 4.7. Plot of Total Pressure Ratio to Mass Flow Rate.

4.3.2 Meshing

One of important aspects of a CFD simulation is effective grid generation. There are different types of grids or meshes available and are classified into structured, unstructured or hybrid grids. Multi-block hexahedral structured grid gives effective grid for a curved surfaces in case of turbomachines. The grid is divided into a structure of blocks known as Topology and Ansys Turbogrid [13] works is the state-of-the-art grid generation tool.

A combination of H/J type of topology is used for upstream and downstreams of the blade. An excellent boundary layer resolution on the blade is obtained by using O-grid topology which forms a continuous loop around the blade profile. Numerical study based on y-plus and number of nodes in the O-grid topology was conducted, where y-plus is the non-dimensional distance from the wall. Since the effect of tur-

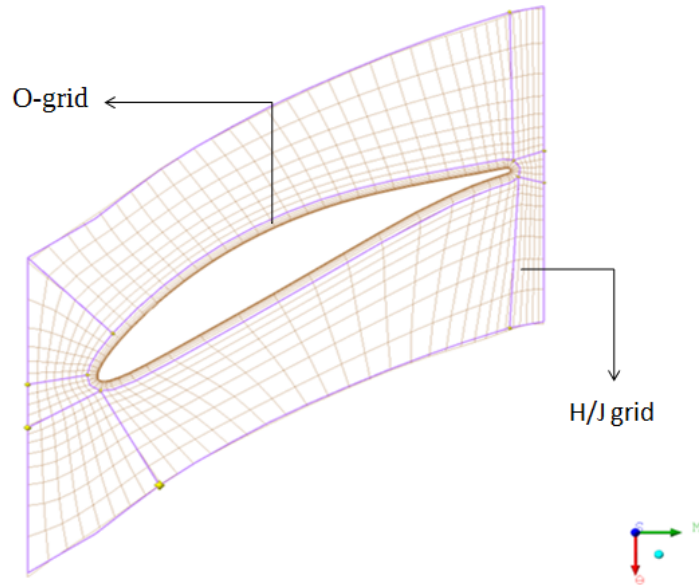


Figure 4.8. Topology at Mid-span of a Rotor.

bulence and boundary layer changes are predominant in regions closer to the blade, the refinement of mesh is carried out in o-grid region. Three nodes are used for each analysis and total time for the simulation is also given. The analysis is carried out using SST turbulence model, which assumes linear wall function at lower y -plus values. The Table 4.2 gives the Total pressure ratio for a set of y -plus values and number of nodes in O-grid. The lower the y -plus value, more resolution of the viscous sublayer is obtained. A y -plus value of 12 is chosen for further analysis since the desired outputs do not much vary from y -plus value of 1 and choosing the former, also lowers computational time and complexity.

4.4 Computational study using three climatic conditions

The Shear Stress Transport as the turbulence model with a y -plus of 12 and number of o-grid elements of 11 for meshing, are used for the analysis of compressor

Table 4.2. Total Pressure ratio and computational time for y-plus values and number of nodes

No. of O-grid Elements (N)	No. of nodes in million	Y-plus 1	Y-plus 12	Y-plus 70	Y-plus 150
11	0.9	3.2334 3.5 hrs	3.2312 3.5 hrs	3.2404 3.5 hrs	3.2471 3.5 hrs
15	1.1	3.2339 3.25 hrs	3.2317 4 hrs	3.2420 4 hrs	3.2477 4.25 hrs
20	1.3	3.2347 4.5 hrs	3.2328 4.5 hrs	3.2431 5 hrs	3.2482 5 hrs
25	1.6	3.2365 4.5 hrs	3.2335 5 hrs	3.2440 5 hrs	3.2480 5 hrs
32	2.0	3.2371 5.5 hrs	3.2347 5.5 hrs	3.2401 5.5 hrs	3.2471 5.5 hrs

for three sets of conditions. The details of the boundary conditions are given in Table 4.3 and outlet Static pressures of 180, 270, 300, 330, 400, 480 are applied for each of the climatic conditions to examine the performance.

Table 4.3. Boundary conditions of 3 climatic conditions

Boundary conditions	Winter	Average	Summer
Inlet total pressure (kPa)	90	89	88
Inlet total temperature (K)	257.15	303.45	281.25
Rotation speed rpm	5100	5100	5100

CHAPTER 5

Results and Discussions

The CFD analysis of the compressor fig 5.1 is carried out. For the Outlet static pressure of 180 kPa, all three climatic conditions are discussed below.

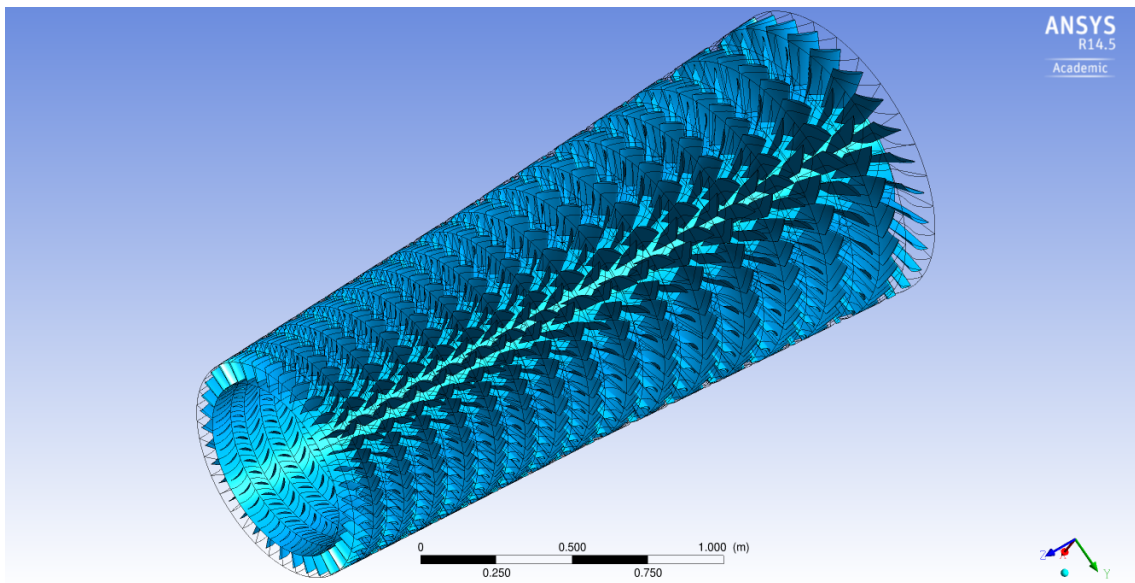


Figure 5.1. 360 degree view of the compressor.

5.1 Outlet Static Pressure of 180 kPa for three climatic conditions

For all three climatic conditions, the residual plots showed a gradual convergence through first 200 iterations, followed by low frequency oscillations. The overall total pressure ratio and inlet mass flow rates are given in Table 5.1. As total temperature increases, a higher inlet mass flow rate is required in order to achieve higher

performance. One way to increase the mass flow rate is by varying stagger angles of the stators.

Table 5.1. Overall Total Pressure ratio and Inlet mass flow rate for three climatic conditions

Climatic conditions	Total Pressure Ratio	Inlet mass flow rate in kg/s
Winter	2.2956	49.5951
Average	2.2760	44.7284
Summer	2.2722	40.9430

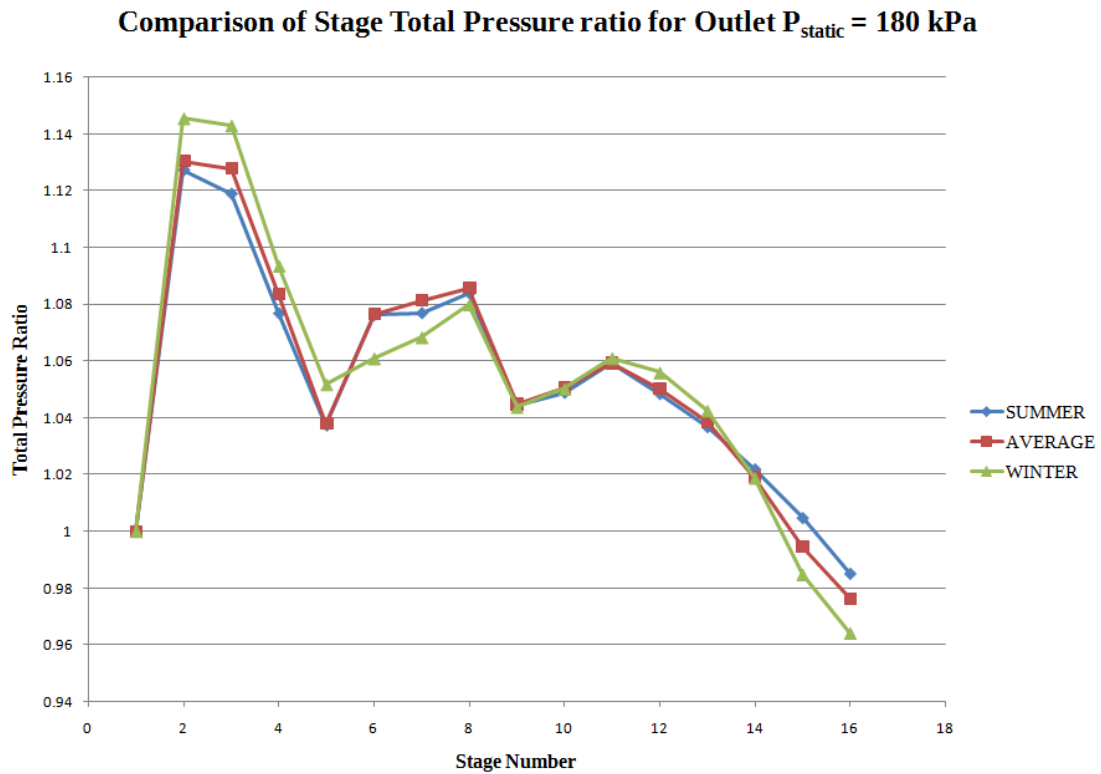


Figure 5.2. Graph of Total Pressure Ratio versus Stage Number.

The fig 5.2 shows plot of Total Pressure ratio versus stage number for all three conditions. For all three conditions, it is seen that variation of total pressure ratio across each stage consistent. The variation of pressure and velocity vectors across the compressor are shown in the figures.

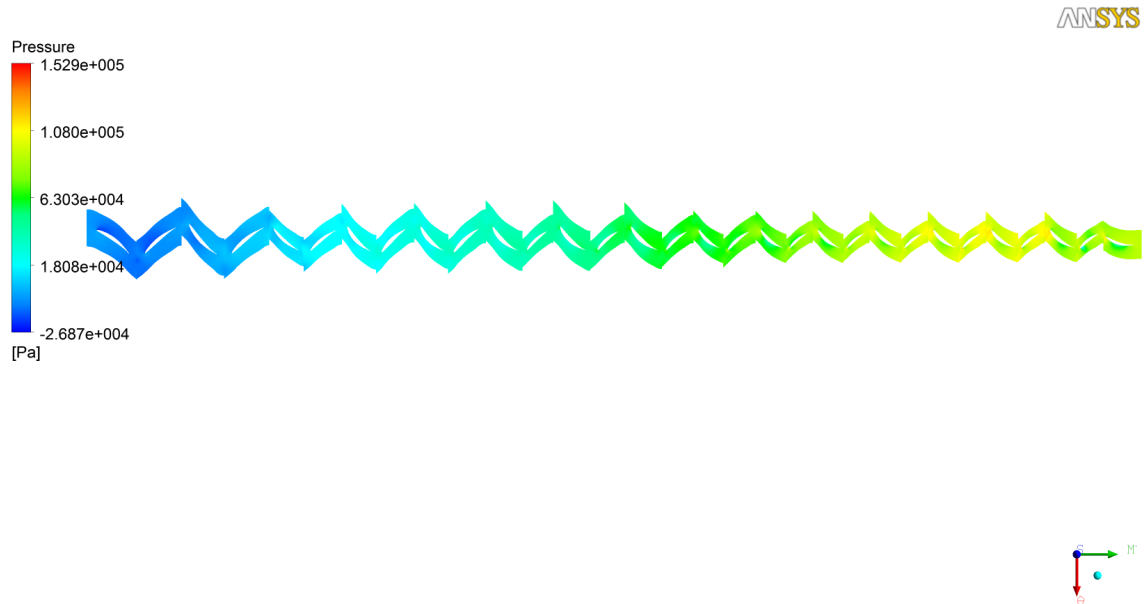


Figure 5.3. Pressure contour at 50 percent mid span for Exit Static Pressure = 180 kPa in winter.

5.2 Outlet Static Pressure of 180 kPa, 270 kPa and 300 kPa for winter condition

Second set of parametric study was carried out for one climatic condition using three outlet static pressures. The fig 5.9 shows variation of total pressure ratio to stage number.

A graph of total pressure ratio versus mass flow rate is presented fig 5.10 for three Static Pressures at exit. Stalling condition was seen when an exit pressure of 330 kPa was used at the exit.

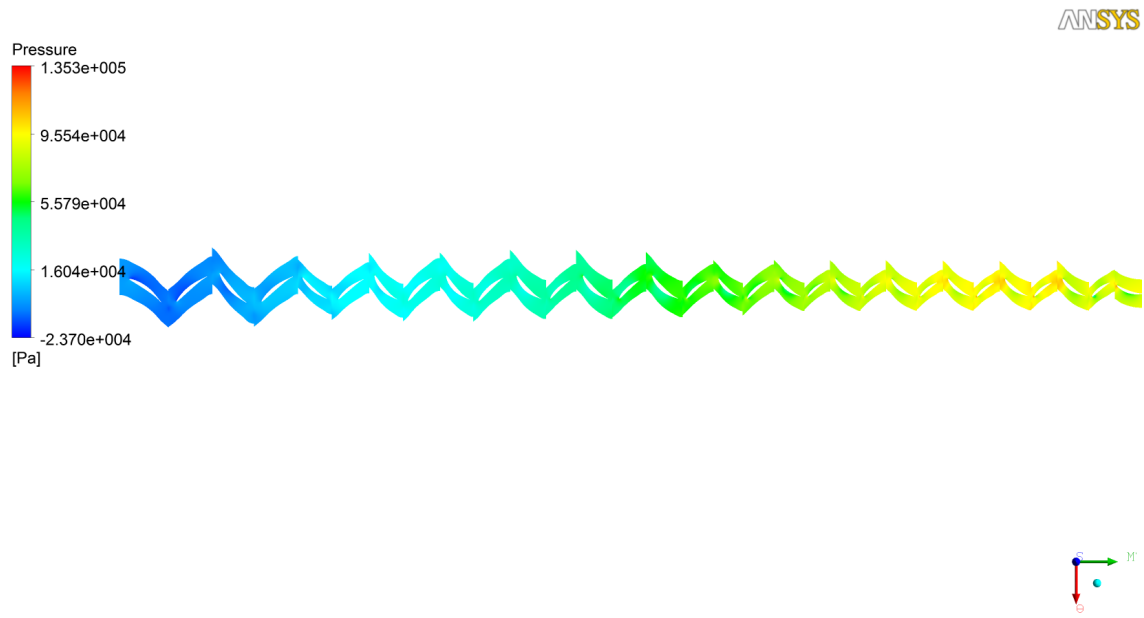


Figure 5.4. Pressure contour at 50 percent mid span for Exit Static Pressure = 180 kPa in average climate.

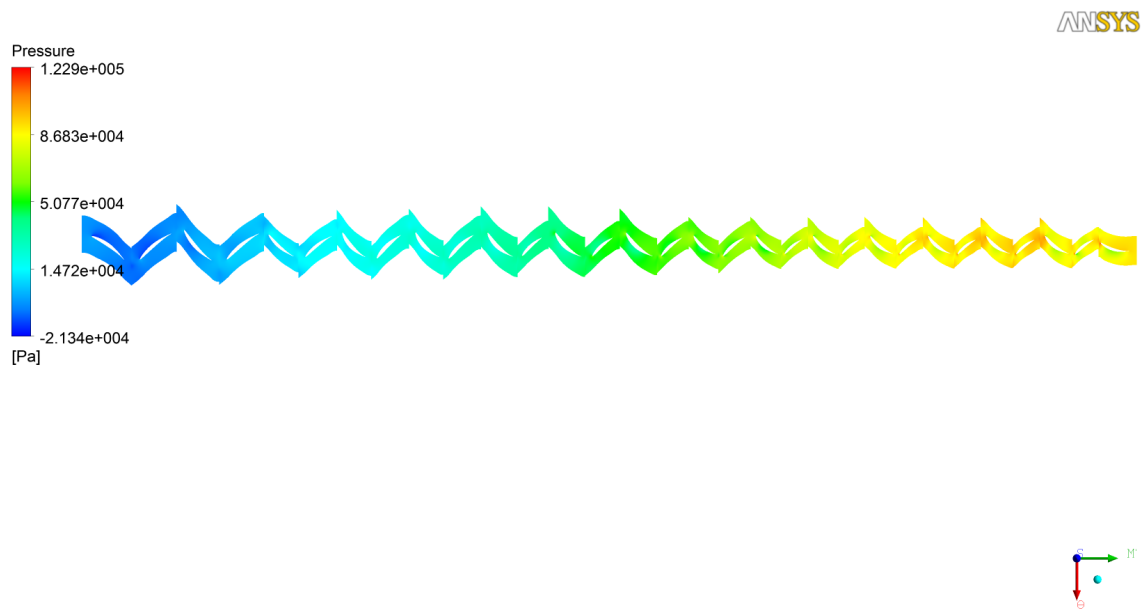


Figure 5.5. Pressure contour at 50 percent mid span for Exit Static Pressure = 180 kPa in summer.

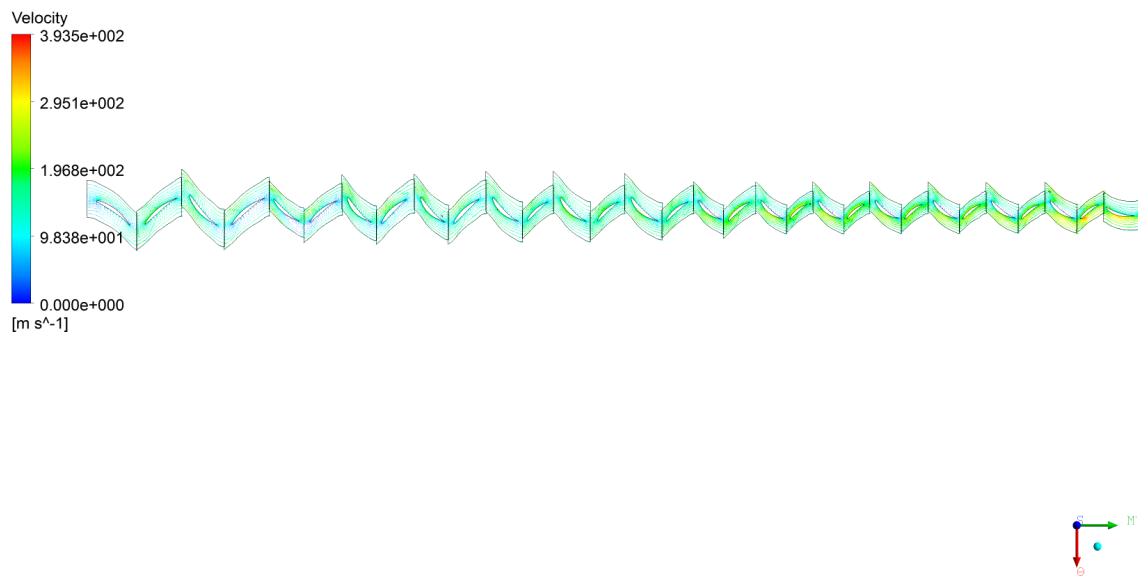


Figure 5.6. Velocity vector plot at 50 percent mid span for Exit Static Pressure = 180 kPa in winter.

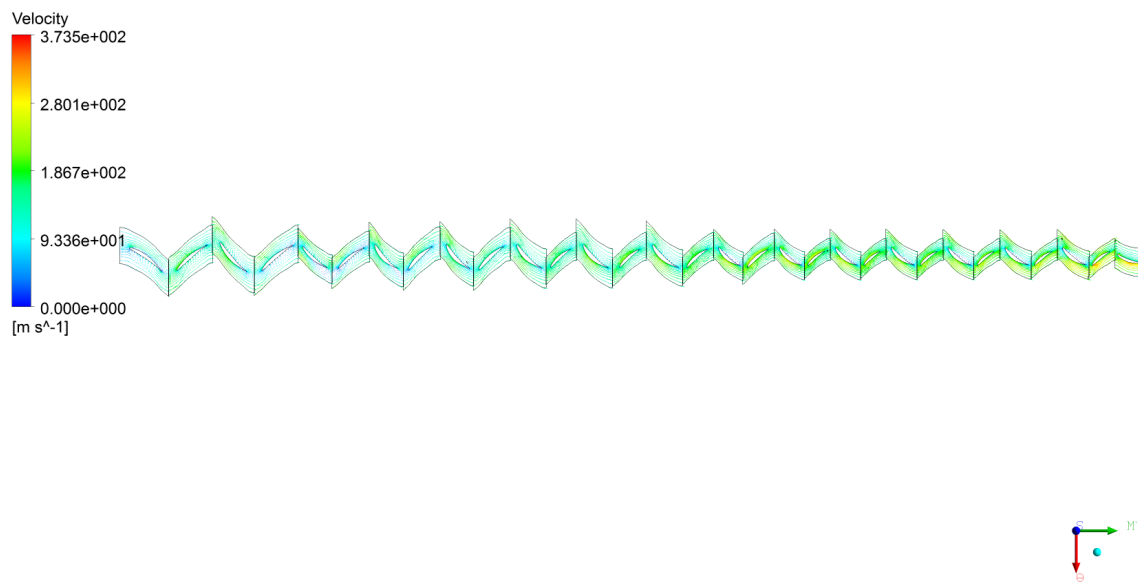


Figure 5.7. Velocity vector plot at 50 percent mid span for Exit Static Pressure = 180 kPa in average climate.

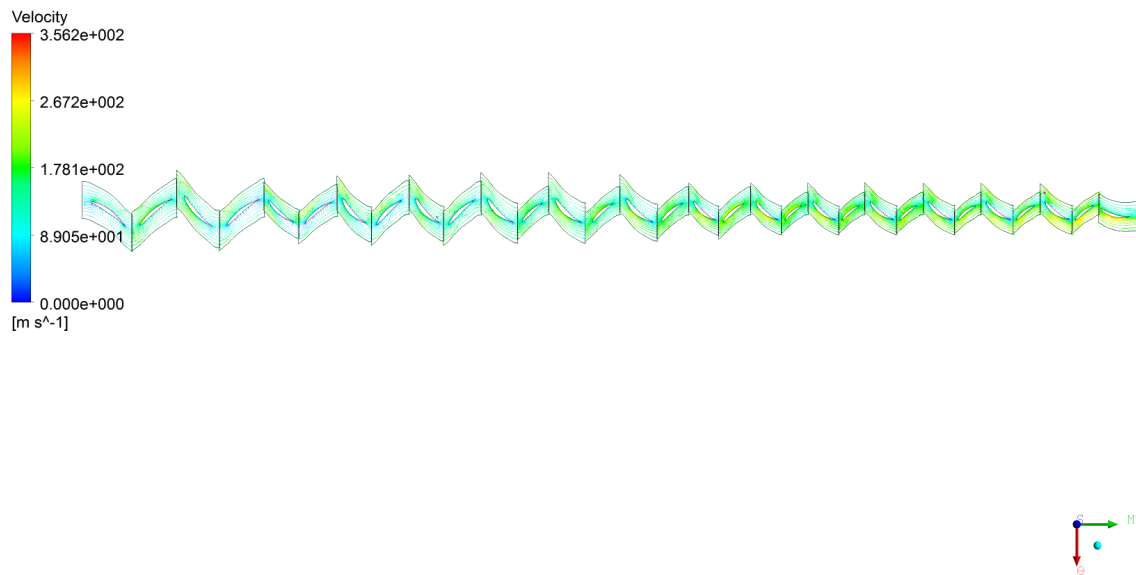


Figure 5.8. Velocity vector plot at 50 percent mid span for Exit Static Pressure = 180 kPa in summer.

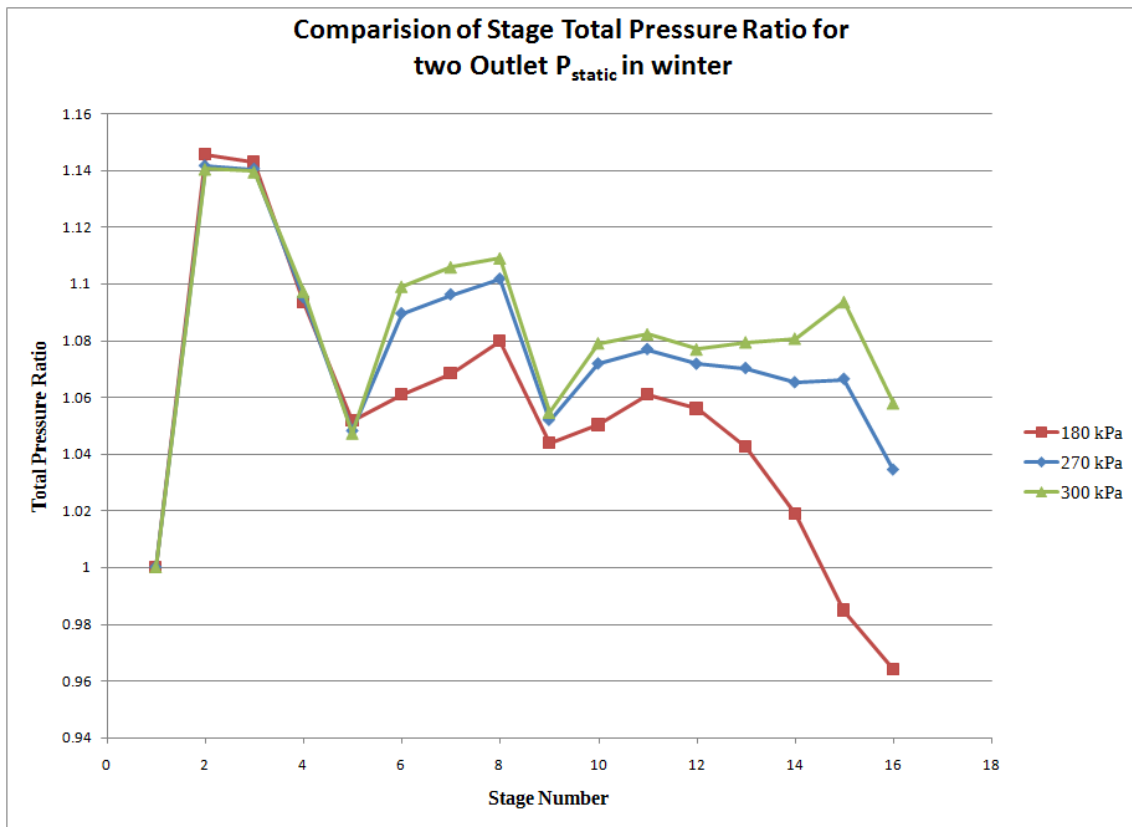


Figure 5.9. Graph of Total Pressure Ratio versus Stage Number for winter condition.

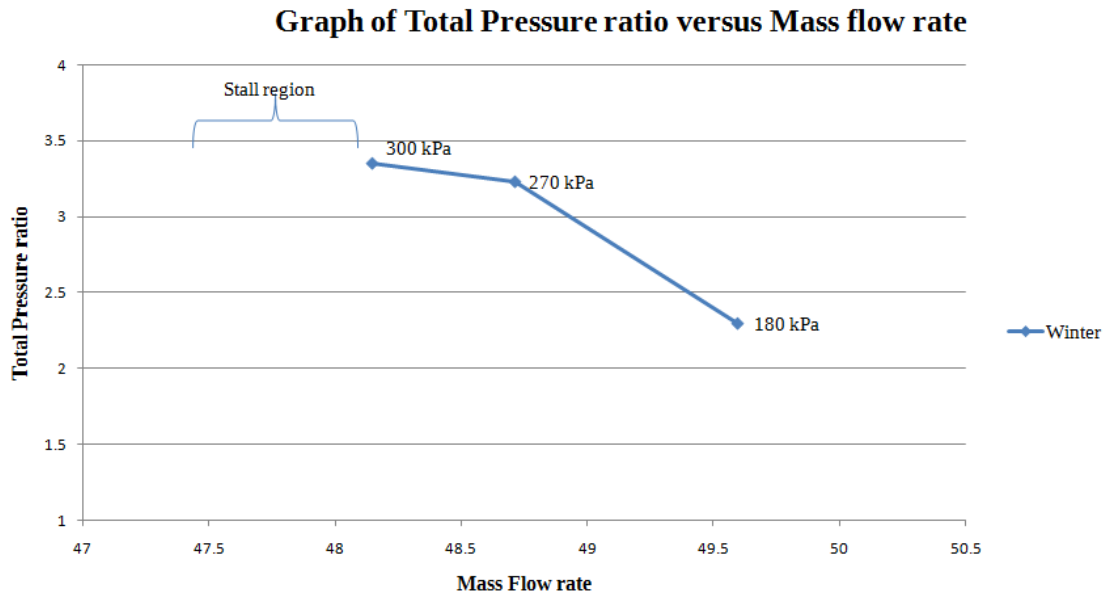


Figure 5.10. Graph of Total Pressure Ratio versus mass flow rate for winter condition.

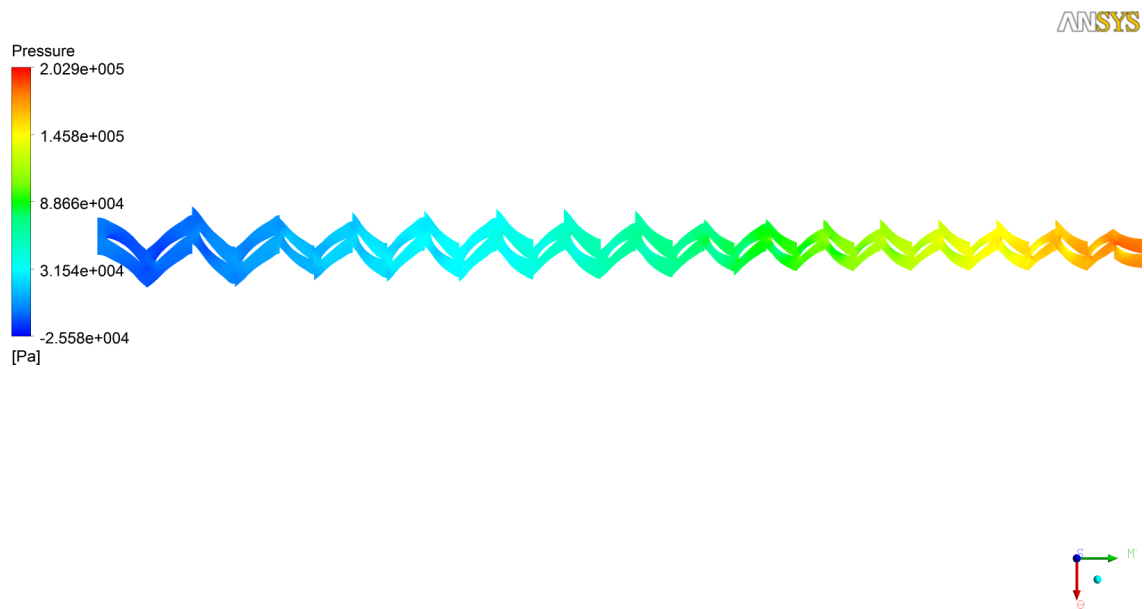


Figure 5.11. Pressure contour at 50 percent mid span for Exit Static Pressure = 270 kPa in winter.

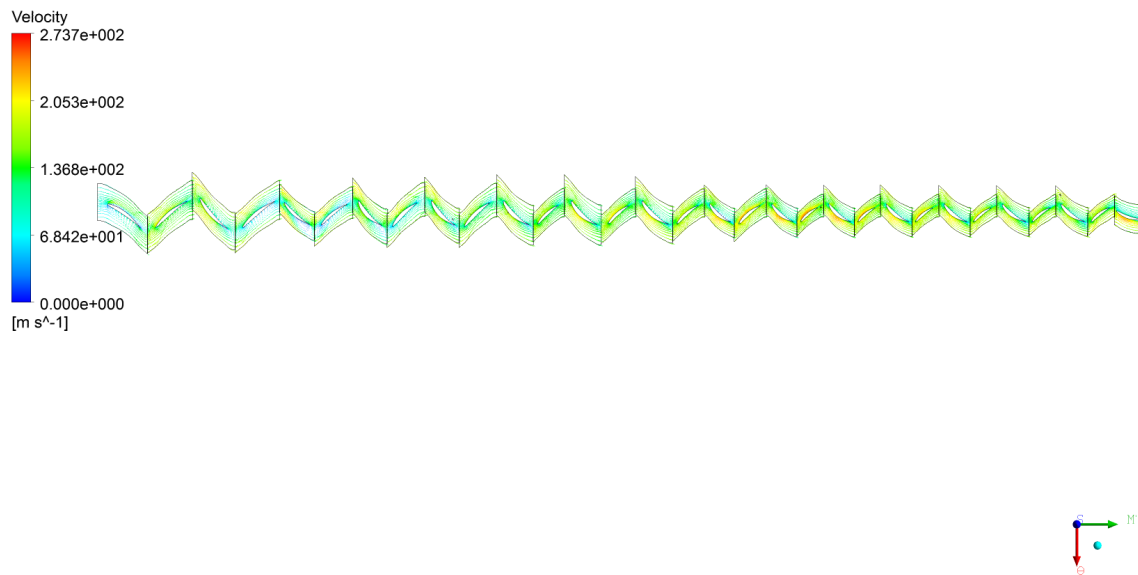


Figure 5.12. Velocity vector plot at 50 percent mid span for Exit Static Pressure = 270 kPa in winter.

CHAPTER 6

Concluding Remarks

This research work presented the parameters that affect computational analysis of a axial flow compressor and its performance. The research was carried out in two segments:

- Preliminary analysis varying certain parameters
- Comparison of performance in two categories

The first segment started with two types of turbulence models, k-epsilon and Shear Stress Transport and their effect on total pressure ratio and mass flow rate. The use of Shear Stress Model showed a 10 percent increase in total pressure ratio. Since SST model showed a notable variation in total pressure ratio for finer grids, this model is concluded to be suitable for the present study. Once the turbulence model is selected, a grid/y-plus sensitivity analysis is carried out by varying y-plus from a value of 1 to 150 and number of nodes from 0.9 to 2 million. For each analysis, wall clock time is observed in order to finalize perfect values, compromising certain results.

Using SST as turbulence model and using a grid with y-plus value of 12 and 0.9 million nodes, a computational analysis is carried out for three climatic conditions and three exit static pressures. The variation of stage total pressure ratio with stage number for exit static pressure of 180 kPa for three climatic conditions is discussed. Analysis using three exit static pressures 180, 270 and 300 kPa for winter condition is graphically presented. The compressor stalling region is highlighted for further improvement in compressor performance.

6.1 Future work

The results of the steady state analysis form base settings for the transient analysis of the compressor. A transient analysis gives in depth knowledge on the onset of flow separation and flow transition between rotor and stator. The range of compressor performance can be further increased by changing the stagger angles of the stators in order to allow more mass flow rate at different climatic conditions.

APPENDIX A
INPUT CODE FOR PARALLEL PROCESSING


```
#!/bin/csh
Batch file for running CFX jobs
start in the directory where the job was
submitted
-cwd
total number of nodes requested(each node has 4 processors)
-l qty.eq.9,quad
name of the job
-N s15ex
commands to be executed
call parallel CFX using 'paracfx' script. Options can be added in quotes.
setenv PATH /usr/bin:PATH
rm -rf /tmp/*.dat /tmp/pvm*
time paracfx " -solver-double -def 15_y12_s15.def "
```

REFERENCES

- [1] C. B. Meher-homji, “The Historical Evolution of Turbomachinery,” 2000.
- [2] T. D. Canonsburg, “ANSYS CFX-Pre User ’ s Guide,” vol. 15317, no. October, pp. 724–746, 2012.
- [3] R. U. E. Ancelle, *CFD Validation for Propulsion System Components (la Validation CFD des organes des propdseurs)*, 1998.
- [4] MIT, “Multistage axial flow compressors.”
- [5] Wikipedia, “Flynn’s taxonomy - Wikipedia, the free encyclopedia.”
- [6] T. D. Canonsburg, “ANSYS CFX-Solver Theory Guide,” vol. 15317, no. October, pp. 724–746, 2012.
- [7] W. Chung-Hua, “ADVISORY COMMITTEE TECHNICAL NOTE 2302,” no. March, 1951.
- [8] J. D. Denton and W. N. Dawes, “Computational fluid dynamics for turbomachinery,” vol. 213, 1990.
- [9] J. C. Tanhill, D. A. Anderson, and R. H. Pletcher, *Computational Fluid Mechanics And Heat Transfer - Anderson.pdf*, 1997.
- [10] T. Jiyuan, Y. Guan Heng, and L. Chaoqun, *Computational Fluid Dynamics: A Practical Approach*. Butterworth-Heinemann, 2008.
- [11] H. Chang, W. Zhao, D. Jin, Z. Peng, and X. Gui, “Numerical investigation of base-setting of stators stagger angles for a 15-stage axial-flow compressor,” *Journal of Thermal Science*, vol. 23, no. 1, pp. 36–44, Jan. 2014. [Online]. Available: <http://link.springer.com/10.1007/s11630-014-0674-x>
- [12] D. D. Knight, “Parallel Computing in Computational Fluid Dynamics.”

- [13] D. Roose and R. V. Driessche, “Parallel Computers and Parallel Algorithms for CFD : An Introduction,” Tech. Rep.
- [14] T. D. Canonsburg, “ANSYS TurboGrid User ’ s Guide,” vol. 15317, no. October, pp. 724–746, 2012.

BIOGRAPHICAL STATEMENT

Chaithanya Mamidoju was born in the city of Nirmal, India in 1991. She obtained a Bachelor's degree in Aeronautical Engineering with a major in Aerodynamics and Propulsion from Jawaharlal Nehru Technological University, Hyderabad in 2012. After graduation she then came to the United States in Fall 2012 to pursue an M.S. degree program in Aerospace Engineering at the University of Texas at Arlington.

Chaithanya has been a Tutor at the UTS for Student Support Services for Undergraduate Students. Her research interests include Computational Fluid Dynamics, Engineering Analysis and Design Optimization. She is currently working in the CFD Lab with Dr. Brian Dennis. She is a student member of AIAA and SWE.